Ceramics International 51 (2025) 65640–65647

Contents lists available at ScienceDirect

Ceramics International

journal homepage: www.elsevier.com/locate/ceramint

Mixed hydro-solvothermal synthesis process: An unconventional route to obtain mixed iron oxide systems

Tatiana Rodríguez Flores [a,1], Falak Shafiq [a,1], Gabriele Bona [a], Giulia Bragaggia [b], Matteo Cantoni [c], Roberto Scotti [a,d], Silvia Gross [b,e], Roberto Nisticò [a,*]

[a] University of Milano-Bicocca, Department of Materials Science, U5, INSTM, Via R. Cozzi 55, 20125, Milano, Italy
[b] University of Padova, Department of Chemical Sciences, Via Marzolo 1, Padova, 35131, Italy
[c] Politecnico di Milano, Department of Physics, Via G. Colombo 81, 20133, Milano, Italy
[d] Institute for Photonics and Nanotechnologies-CNR, Via alla Cascata 56/C, 38123, Povo, (TN), Italy
[e] Karlsruher Institut für Technologie (KIT), Institut für Technische Chemie und Polymerchemie (ITCP), Engesserstr. 20, Karlsruhe, 76131, Germany

ARTICLE INFO

Keywords:
Hematite
Hydrothermal synthesis
Iron oxides
Magnetic properties
Magnetite
Solvothermal synthesis

ABSTRACT

The present study explores a new mixed hydro-solvothermal protocol for the synthesis of iron oxide-based materials at relatively mild conditions (150 °C), by selecting different water/2-propanol mixtures as reaction environments, and NaOH as a precipitating agent. Syntheses were performed in the absence of any structure directing agents and reducing agents, employing directly a mixture of Fe(II) and Fe(III) salts as iron oxide precursors. Morphological, structural, and magnetic variations of the resulting materials were monitored by means of scanning electron microscopy (SEM), X-ray powder diffraction (XRPD), and vibrating sample magnetometry (VSM) characterizations. Experimental results demonstrated the influence of the composition of the reaction medium on the crystal phase composition, morphology, and magnetic response. In particular, syntheses carried out at a high water/2-propanol volume ratio observed the predominant formation of the magnetite (Fe_3O_4)/maghemite (γ-Fe_2O_3) crystal phase, whereas the low water/2-propanol volume ratio favored the formation of the hematite (α-Fe_2O_3) crystal phase, thus outlining the important role played by the solvent mixture composition in directing the particles' nucleation, growth, and agglomeration. Furthermore, magnetic measurements demonstrated a direct correlation existing between the synthesis conditions (and consequently the crystal phase compositions) and the observed magnetic properties, recording an increase of the magnetization along with the content of the magnetite/maghemite crystal phase. These results demonstrated that with this mixed hydro-solvothermal protocol it is possible to finely tailor both structural and functional properties of iron oxide-based materials by simply varying the synthesis conditions, thus providing valuable insights for the rational design of mixed phase materials.

1. Introduction

Currently, iron oxide-based materials have gained significant interest due to their low cost, natural availability, exceptional magnetic properties, chemical stability, and versatility in numerous technological applications, such as in environmental remediation [1–5], (photo) catalysis [6–8], sensing [9], biomedicine [10–12], magnetic resonance imaging [13,14], and drug-delivery systems [15,16]. Among this class of materials, magnetite (*i.e.*, the mixed ferrous-ferric oxide crystal phase, Fe_3O_4), maghemite (*i.e.*, the ferrous-deficient magnetite isometric crystal form, γ-Fe_2O_3), and hematite (*i.e.*, the most thermodynamically stable iron oxide crystal form, α-Fe_2O_3) are the main relevant crystal forms [17]. These materials exhibit a range of magnetic behaviors, such as either ferrimagnetism (Fe_3O_4/γ-Fe_2O_3), antiferromagnetism (α-Fe_2O_3), superparamagnetism (depending on the particles' size), or paramagnetism (depending on the operational temperature), making them ideal candidates in many emerging technologies.

The magnetic properties of these iron oxide-based materials can be significantly influenced by morphological (*e.g.*, particles' size, shape, anisotropy, aspect ratio) [18] and compositional (*e.g.*, purity, doping)

* Corresponding author.
E-mail address: roberto.nistico@unimib.it (R. Nisticò).
[1] Both authors contributed equally to this work.

https://doi.org/10.1016/j.ceramint.2025.11.241
Received 21 September 2025; Received in revised form 13 November 2025; Accepted 17 November 2025
Available online 17 November 2025

[19] features, which are strongly influenced by the different synthesis conditions [20]. Among the different chemical strategies to prepare them, soft chemistry approaches, and in particular hydrothermal and solvothermal routes, are very appealing synthesis methods for their ability to pursue a high morphology-control in the production of inorganic materials at relatively mild conditions (below 200 °C) [21]. In this context, both hydrothermal and solvothermal routes are synthesis strategies that involve the use of solvents (either water or organic solvents, respectively) above their boiling points in a sealed vessel, with the development of autogenous pressure, which depends on the filling ratio of the vessel. Under these experimental conditions, even whenever the reaction mixture does not reach the supercritical point, the changes in the solvent properties in response to the increased temperature and pressure (with decrease of the dielectric constant, viscosity, and density) increase the solvating power of the dispersing phase, allowing for the solubilization of compounds that would normally be insoluble, but also disclose unusual crystallization pathways with respect to the ones occurring under normal conditions, with the possibility of directly obtaining metastable crystalline phases, without the necessity of performing a further annealing treatment [22,23].

According to the literature, both solvents' nature and composition (*i.e.*, volume ratio) are among the main parameters influencing the composition, crystal phase, morphology, and, consequently, the magnetic response of the final products [24]. Indeed, in the case of mixtures of solvents, by adjusting the volume ratios of the solvents' mixture, it is possible to tune the formation of particles with uniform size distribution, optimal magnetic properties, and enhanced surface reactivity. However, even if it is well-known that mixtures of solvents affect both the viscosity and the dielectric constant of the reaction medium, leading to the nucleation and growth of completely different materials, only a few studies investigated the possibility of using mixed hydro-solvothermal routes [23,25–27]. In particular, in our previous study [23], we investigated the role of compositional parameters on the synthesis of different anisotropic magnetic materials following a mixed hydro-solvothermal route in the presence of a water/2-propanol mixture, employing poly (ethylene glycol) as a structure-directing agent, sodium thiosulfate as a reducing agent, and NaOH as a precipitating agent, finding a correlation between the reaction medium composition and the final materials' crystal phase, morphology, and magnetic response. The obtained results indicated that syntheses performed in water/PEG and 2-propanol/PEG environments favor the formation of magnetite phases (with nanorods in the case of water/PEG environment and polyhedral morphologies in the case of the 2-propanol/PEG environment) with only traces of hematite (in lamellar shape), whereas syntheses performed in mixed water/2-propanol/PEG environments favor the growth of the hematite phase. In all cases, magnetic characterization evidenced a superparamagnetic behavior, with higher saturation values in the case of samples predominantly made by the magnetite phase (*ca.* 41–52 emu g^{-1}) compared to the ones predominantly made by hematite (*ca.* 4–14 emu g^{-1}), which results being very weak magnetic.

In this context, the possibility of modulating the magnetic response of iron oxides mixtures by simply varying the phase composition through the aprioristic selection of the reaction environment is of great interest for the design of always novel, environmental benign and energy efficient synthesis processes.

Hence, in the present study, a new mixed hydro-solvothermal protocol for the synthesis of iron oxide-based materials was explored, working at mild conditions (150 °C), using a mixed water/2-propanol reaction medium (varying the volume ratio between the two solvents), and using NaOH as a precipitating agent. In particular, the term "*mixed hydro-solvothermal synthesis*" refers to the combination of aqueous (hydrothermal) and organic (solvothermal) environments achieved by employing a mixture of miscible solvents (*i.e.*, water and 2-propanol) able to generate a reaction environment with intermediate properties respect to the two pure solvents (*e.g.*, different polarity and redox character). Compared to our previous study [23], in this case, syntheses were performed in the absence of any structure directing agents and reducing agents, employing directly a mixture of Fe(II) and Fe(III) salts as iron oxide precursors. Since the proposed synthesis operates at moderate temperature, avoid the use of toxic reagents, as requires only water and 2-propanol as solvents, and abundant Fe(II) and Fe(III) salts as iron oxides' precursors, without the need of any external reducing agent, the mixed hydro-solvothermal route here proposed is fully compliant with the principles of green chemistry. Morphological, structural, and magnetic variations of the resulting materials were monitored by means of scanning electron microscopy (SEM), X-ray powder diffraction (XRPD), and vibrating sample magnetometry (VSM). Correlations between the different operational conditions and the samples' morphological, chemical, and magnetic characteristics are presented, and trends are critically discussed.

2. Experimental

2.1. Chemicals

Fe(II) chloride tetrahydrate ($FeCl_2 \bullet 4H_2O$, CAS 13478-10-9, Merck), Fe(III) chloride hexahydrate ($FeCl_3 \bullet 6H_2O$, CAS 10025-77-1, Merck), and sodium hydroxide pellets (NaOH, CAS 1310-73-2, ACS reagent, ≥98 %, Merck), 2-propanol (C_3H_8O, anhydrous, CAS 67-63-0, 99.5 %, Sigma-Aldrich), acetone (C_3H_6O, CAS 67-64-1, Sigma-Aldrich). Furthermore, deionized Milli-Q water with a resistivity of 18.2 MΩ cm was used. All chemicals were employed as received, without further purification.

2.2. Hydro-solvothermal synthesis

Iron oxides were prepared following a properly modified procedure taken from the literature [28]. In a typical synthesis, Fe(II) chloride tetrahydrate (0.05 M) and Fe(III) chloride hexahydrate (0.10 M) were dissolved in a mixture of water and 2-propanol (considering a total volume of 40 mL), maintaining constant the Fe^{2+}:Fe^{3+} 1:2 molar ratio and varying the water:2-propanol volume ratio, namely: 100/0, 75/25, 50/50, 25/75, 0/100 v/v. The aqueous component was not deoxygenated prior to synthesis, thus allowing dissolved oxygen to remain in the reaction medium. Subsequently, an alkaline solution (2 M NaOH, 10 mL) was added dropwise under magnetic stirring, thus reaching the final volume of 50 mL. The final solution was transferred into a 150 mL PTFE vessel, which was then sealed in a Berghof stainless steel Acid-Digestion Bomb (reaching a filling ratio of 33.3 %) and heated at 150 °C for 24 h. Afterwards, the reactor was left to cool down naturally to room temperature (RT). The iron oxide particles were collected by centrifugation (12,000 rpm, 3 min) and washed (three times with deionized water and one time with acetone) to remove impurities. Lastly, samples were oven-dried under air atmosphere at 70 °C overnight and grinded before storing. The synthesized samples were labeled as WXPY (where X and Y refer to the % volume ratio of both water and 2-propanol, respectively). A schematic representation of the mixed hydro-solvothermal route here investigated is reported in Fig. 1.

2.3. Characterization

Scanning Electron Microscopy (SEM) micrographs were collected by means of a Zeiss Gemini 500 microscope equipped with a traditional secondary electron detector (5 kV). Samples were deposited onto SEM stubs using a double-adhesive carbon tape, then they were covered with Au coating to prevent charging effects using a VPI SD-900C sputter coater.

X-Ray Powder Diffraction (XRPD) patterns were collected by means of a Rigaku Miniflex 600 with a Cu source working at 40 kV and 15 mA, scanning in a range of 10–80° 2θ with a size step of 0.02°, and an angular velocity 5.0° per minute. XRD patterns were indexed according to the ICDD database using the instrumental PDXL-2 software.

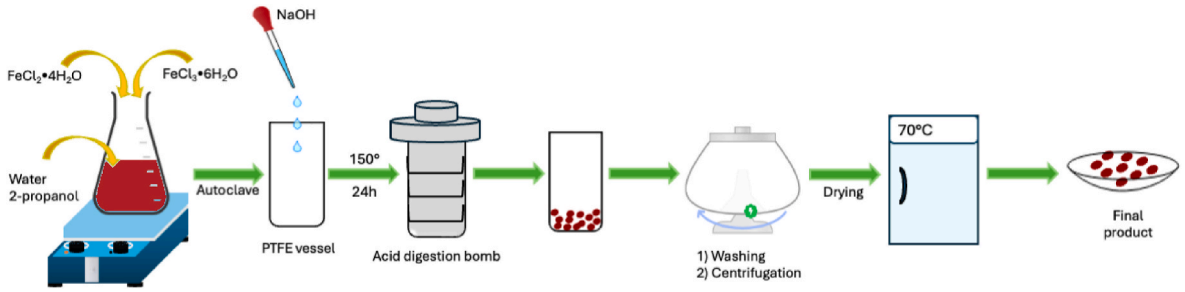

Fig. 1. Schematic representation of the mixed hydro-solvothermal route employed for the synthesis of iron oxide-based materials.

The crystallite average size was estimated by means of the Scherrer equation (Eq. (1)):

$$\tau = \frac{K\lambda}{\beta \cos\theta} \quad (1)$$

where τ is the average size of the crystalline domains (expressed in nm), K is the shape factor (typically 0.9), λ is the X-ray wavelength (0.154 nm for a Cu source), β is the line broadening at half the maximum intensity (FWHM) of the selected Bragg angle after subtracting the instrumental line broadening (expressed in radians), and θ is the Bragg angle (expressed in radians). For the magnetite/maghemite (Fe_3O_4/γ-Fe_2O_3) crystal phase, the Bragg angle selected is the crystal reflection at 30.4° 2θ (corresponding to the Miller index (220)), whereas for the hematite (α-Fe_2O_3) crystal phase, the Bragg angle selected is the crystal reflection at 33.2° 2θ (corresponding to the Miller index (104)).

The lattice parameters were calculated using the instrumental PDXL-2 software.

The quantitative analysis of the content in magnetite/maghemite and hematite within the samples was calculated by means of the following equation (Eq. (2)), analogously as in Mahadevan et al. [29]:

$$W_m = \frac{I_m}{I_m + I_h} \quad (2)$$

where W_m is the weight percentage of magnetite/maghemite, I_m is the intensity of the magnetite/maghemite phase, and I_h is the intensity of the hematite phase. Since the intensity of a Bragg peak is directly proportional to the area under the curve representing the diffraction intensity, it is possible to calculate the percentage of each phase by using the area under the curve. Therefore, a higher area under a Bragg peak indicates a greater corresponding phase present in the sample [30,31].

Vibrating Sample Magnetometry (VSM) magnetization curves were obtained by using an EZ-9 MicroSense Magnetometer, with a resolution of 1 μemu and maximum field of 2.25 T. Measurements were performed at RT, using quartz cuvettes as sample holders. The magnetic contribution from the cuvettes was measured separately by running baseline correction, placing an empty cuvette, and being automatically subtracted as a diamagnetic background by the instrumental software. The absence of any spurious ferromagnetic contribution from the cuvettes was verified before any measurements.

3. Results and discussion

3.1. Morphological and structural characterizations

The effect of the reaction environment on the final morphology of the synthesized nanomaterials was studied by means of SEM analysis. As shown in Fig. 2A, when pure water was used as the reaction environment (W100P0), the resulting sample exhibited a bimodal distribution of particles, characterized by the presence of both small, irregular shaped flake particles (average size: *ca.* 46 ± 11 nm) organized into large agglomerates and the presence of long anisotropic structures (average thickness: *ca.* 2.28 ± 0.98 μm). According to the literature, the occurrence of agglomerated nanoparticles can be attributed to the growth of the magnetite/maghemite phase (*vide infra*) [32,33], whereas the occurrence of large anisotropic structures might be associated with the formation of the hematite phase (*vide infra*) [34,35]. In contrast, as shown in Fig. 2B, when pure 2-propanol was used as reaction environment (W0P100), the resulting sample presented the formation of less defined structures with an overall morphology appearing more irregular and fragmented (average size: *ca.* 27 ± 4 nm), thus indicating that water and 2-propanol promoted a different crystallization pathway [36]. In particular, it is well known that water and 2-propanol have a different polarity and different dielectric constants (with the relative dielectric constant equal to 80.1 for water and 17.9 for 2-propanol at 20 °C), and that solvent polarity plays a crucial role in driving the growth of specific anisotropic structures as well as specific crystal phases [37,38]. As reported by Pawar et al. [38], and according to Modeshia et al. [39],

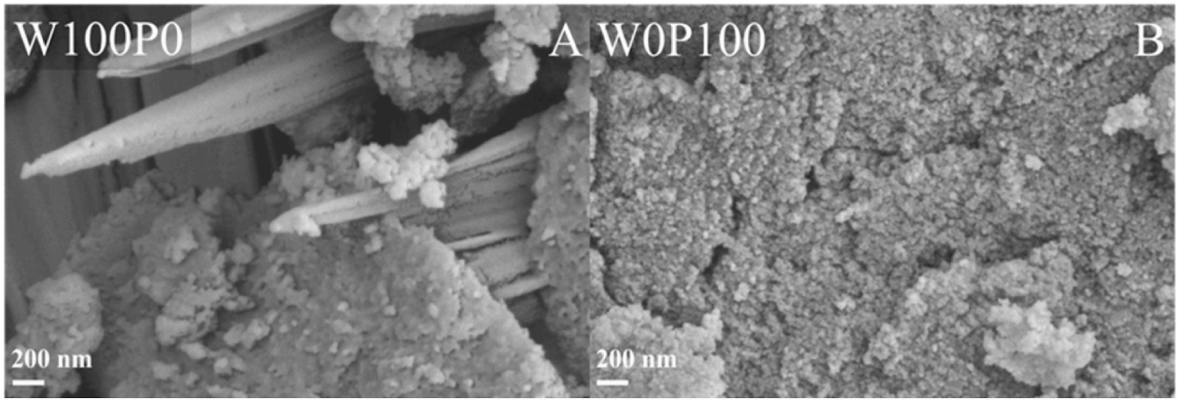

Fig. 2. SEM micrographs of iron oxide-based samples obtained in pure water environment, W100P0 (A, left), and pure 2-propanol environment, W0P100 (B, right). Micrographs were collected at 75*k* × magnifications.

typically hydro/solvothermal growth processes involve a dissolution/precipitation two-step mechanism, with: (i) *in situ* transformation (step 1) in which the precursor ions are dissolved in the reaction mixture from nanoparticles to tiny quantities of the target compound (as solutes) in the liquid phase, followed by (ii) diffusion, precipitation, and growth (step 2) due to the low solubility of the final compound, even at high pressure and temperature, with consequent occurrence of crystal growth. In particular, under hydrothermal conditions, the rapid dissolution of both precursors and precipitating agents (with increment of alkalinity) is facilitated by the polar nature of the reaction medium. Moreover, the polarity of water also promotes the formation of large particles [40]. On the contrary, in the case of the solvothermal synthesis performed in pure 2-propanol, the solubility of both precursors and the precipitating agent is reduced, thus decreasing the hydrolysis of Fe ions in the medium during the growth process and consequently favoring the formation of a large number of tiny nanostructures.

Interestingly, by performing the synthesis in mixed hydro-solvothermal environments and by varying the water/2-propanol ratio, significant changes in terms of final morphology were observed. In particular, in the case of the synthesis carried out in a mixed water/2-propanol reaction environment, with the high water/2-propanol volume ratio (W75P25), the resulting sample was primarily constituted by the co-presence of large lamellar systems (average thickness: *ca.* 1.70 ± 0.51 μm) and large agglomerates composed of small irregular shaped flake particles (average size: *ca.* 29 ± 7 nm; Fig. 3A). In the case of an equal volume ratio between water and 2-propanol (W50P50), a more uniform distribution of the particles seemed to be favored, thus leading to a more isotropic shape of the small nanoparticles (average size: *ca.* 38 ± 10 nm; Fig. 3B). Lastly, in the case of the synthesis performed in a mixed water/2-propanol reaction environment with a low water/2-propanol volume ratio (W25P75), the resulting sample exhibited a lower agglomeration degree, with the formation of large platelets (average size: *ca.* 128 ± 60 nm) together with the agglomerates composed of small irregular shaped flake particles (average size: *ca.* 37 ± 4 nm; Fig. 3C).

These results demonstrated that performing the synthesis in a mixed water/2-propanol environment affected the morphology of the resulting iron oxide-based materials, thus indicating different nucleation and growth processes. In particular, Pawar et al. [38] reported that working in a mixed environment can favor moderate growth kinetics during the hydro/solvothermal process. Again, the hydrolysis of Fe ions initiates the nucleation process, and the formation of large particles (as in W75P25 and in W25P75) is usually obtained by Ostwald ripening processes [41].

The effect of the reaction environment on the crystal structure and iron oxide crystal phase distribution was monitored by means of XRPD analysis. In particular, the XRPD patterns displayed in Fig. 4 revealed in all samples the co-presence of the main crystal reflection planes attributable to both the magnetite/maghemite phase (cubic structure, space group $Fd\underline{3}m$) at 2θ = 30.36° (220), 35.77° (311), 43.47° (400), 53.95° (422), 57.51° (333), 63.17° (440), and 66.42° (531) (JSPDS card no. 01-074-0748), and the hematite phase (trigonal structure, space group $R\underline{3}c$) at 2θ = 24.14° (012), 33.15° (104), 35.61° (110), 40.86° (113), 49.48° (024), 54.09° (116), 57.43 (122), 62.45 (214), and 63.99° (300) (JSPDS card no. 01-089-8104). Furthermore, since both magnetite and maghemite phases have similar crystal structures, it is difficult to distinguish them by applying XRPD technique. On the other hand, it is well known that magnetite can easily transform into maghemite through a topotactic oxidation process, in which the original crystal orientation is preserved [23].

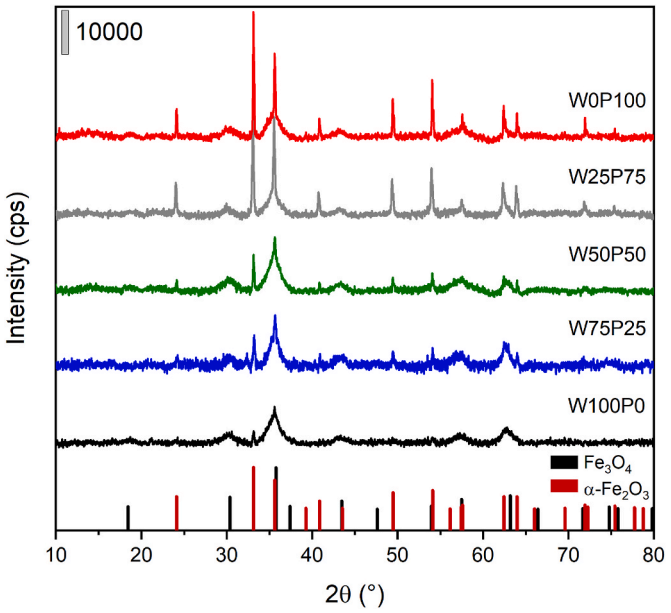

Fig. 4. XRPD patterns of samples obtained in pure water environment, pure 2-propanol environment, and mixed water/2-propanol environment, varying the water/2-propanol volume ratio, namely: W100P0 (black), W75P25 (blue), W50P50 (green), W25P75 (grey), W0P100 (red). XRPD reference patterns: magnetite (01–074–0748, Fe_3O_4, black), and hematite (01–089–8104, α-Fe_2O_3, red). (For interpretation of the references to colour in this figure legend, the reader is referred to the Web version of this article.)

Table 1 reports the quantitative analysis relative to the two recognized crystal phases (*i.e.*, magnetite/maghemite and hematite), the lattice parameters, and the crystallite size calculated by employing the Debye-Scherrer equation. The results indicated a preferential formation of either magnetite/maghemite or hematite phases depending on the solvent of the reaction and, in particular, related to the water/2-propanol volume ratio. In the case of pure water environment (W100P0 sample), a prevalence of the magnetite/maghemite phase was observed (*ca.* 70 wt%) with respect to hematite (*ca.* 30 wt%), whereas opposite behavior was observed for the synthesis with pure 2-propanol environment (W0P100 sample), with a higher presence of hematite (*ca.* 56 wt%) with respect to the magnetite/maghemite crystal phase (*ca.* 44 wt%). Furthermore, by working under mixed solvents environment, and

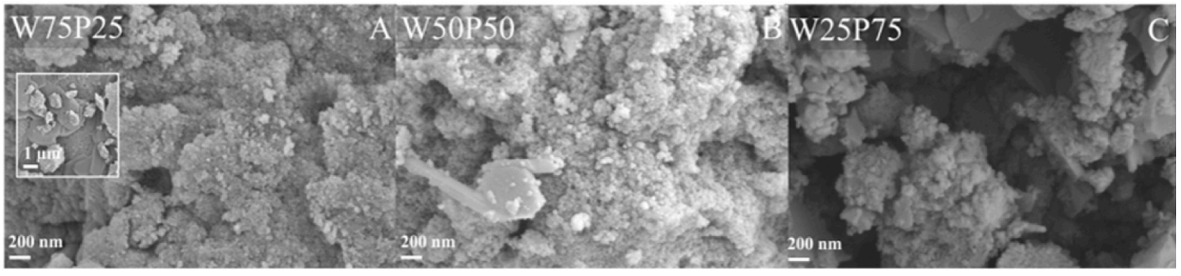

Fig. 3. SEM micrographs of samples obtained in mixed water/2-propanol environment, varying the water/2-propanol volume ratio, namely: W75P25 (A, left), W50P50 (B, middle), and W25P75 (C, right). Micrographs were collected at 75k × magnifications. Inset in Panel A was collected at 10k × magnification.

Table 1
Quantitative analysis estimated by means of Eq. (2), lattice parameter calculation, and average crystallite size dimensions estimated by means of Eq. (1) for the two crystal phases present in the samples, namely: magnetite/maghemite, and hematite.

Sample	Phase percentage (wt.%)		Lattice parameters			Average crystallite size (nm)	
			Magnetite/Maghemite	Hematite			
	Magnetite/Maghemite	Hematite	a = b = c (Å)	a = b (Å)	c (Å)	Magnetite/Maghemite	Hematite
W100P0	70	30	8.35	5.02	13.78	9	70
W75P25	62	38	8.36	5.07	13.67	8	75
W50P50	66	34	8.32	5.04	13.76	7	85
W25P75	57	43	8.32	5.03	13.74	11	60
W0P100	44	56	8.34	5.03	13.74	8	85

in particular by gradually reducing the water/2-propanol volume ratio, a progressive increment of the hematite phase content was observed (as quantified in Table 1). Explaining this behavior is challenging, as there are several factors that influence both the preferential crystal phase formation as well as the particles' morphology and aggregation level.

However, the collected experimental results summarized in Table 1 demonstrated that in the mixed hydro-solvothermal conditions, both solvents' nature and volume ratio played a key role in the preferential formation of one crystal phase over the other one. In particular, this trend can be explained by considering some distinctive properties of the solvent mixture and the interaction with the metal ion precursors. As previously discussed, water is a highly polar solvent (Rohrschneider's polarity parameter, P' = 10.2) compared to 2-propanol (P' = 3.9) [42], and polarity plays a crucial role in these interactions. Lu et al. [43] demonstrated that in the solvothermal synthesis of titania nanoparticles, the solvent polarity index of the reaction medium plays a crucial role not only in tuning size and shape but also in determining nanomaterials' crystal phase. Polar solvents (*e.g.*, ethanol) tend to favor the formation of the anatase crystal phase, whereas solvents with moderate-low polarity favor the formation of the rutile crystal phase.

Another important parameter is the solvation effect, which varies with the solvent's nature. In fact, in water/aqueous environment, the solvation through hydrogen bonding with hydroxyl groups partially shields hydroxy ions, thus causing a decrease of their activity, whereas in 2-propanol environment, the solvation effect is weaker than in water, thus inducing a higher hydroxyl ion activity (and consequently making the environment more oxidizing) [24,44]. As reported by Demazeau [24], the chemical reactivity of hydroxyl ions in a solvothermal alcoholic environment is improved compared to the hydrothermal water environment.

Furthermore, the replacement of magnetite/maghemite with the hematite crystal phase under mild hydrothermal conditions is a natural phenomenon occurring below the terrestrial crust through either redox or non-redox processes [45]. In the latter case, mainly through Fe^{2+} leaching from the magnetite crystal phase via the action of solution parameters, it influenced both the solubility of magnetite crystal phase and the transport of Fe^{2+} ions (*e.g.*, pH, concentrations of ligands) [45].

Therefore, by considering all these parameters together, when pure 2-propanol was used as a reaction medium, the formation of hematite crystal phase was consequently favored due to the reaction environment tendency to facilitate the nucleation and growth of the fully oxidized Fe^{3+} species [35]. On the other side, in the case of systems synthesized under mixed water/2-propanol conditions, the balance between all these phenomena drives the crystal phase composition toward the predominance of magnetite/maghemite crystal phase with respect to the hematite one.

In this regard, it should be highlighted that Satheesh et al. [46] reported the growth of hematite nanoparticles with different morphology and size by employing different mixed hydro-solvothermal environments (*i.e.*, methanol, methanol-water, propanol, and propanol-water), whereas An et al. [47] reported the template-free synthesis of hematite nanoparticles through mixed hydro-solvothermal process by using an ethanol:water (9:1, v/v) mixture. Although the exact roles played by the organic solvent (ethanol in this case, 2-propanol in our case) was not clear, An et al. [47] proposed that ethanol might act both as solvent and complexation agent forming an initial iron alkoxide precursor able to stabilize Fe^{3+} ions of hematite crystal phase.

The lattice parameters of the two crystal phases forming in all samples are reported in Table 1, with almost negligible lattice variations registered between the different samples. In fact, in the case of the trigonal hematite crystal phase, it is not possible to find a well-defined correlation attributable to the lattice parameter variations. The W100P0 sample exhibited the lowest values in terms of both *a* and *b* parameters and the largest one in terms of *c* parameter, and W75P25 sample exhibited the largest values in terms of both *a* and *b* parameters and the lowest in terms of the *c* parameter. By increasing the content of 2-propanol, all three cell parameters remain almost constant with intermediate values with respect to the ones highlighted in the previous samples. In the case of the cubic magnetite/maghemite crystal phase, the largest lattice parameters were registered for W75P25, and the lowest were observed with further increase in the 2-propanol content (*i.e.*, W50P50 and W25P75).

Regarding the average crystallite sizes of both magnetite/maghemite and hematite crystal phases within the iron oxide samples, these values were determined by means of applying the Debye-Scherrer equation considering the diffraction peaks at 30.4° and 33.2°, respectively. As shown in Table 1, the average crystallite sizes calculated for the magnetite/maghemite crystal phase followed the previously evidenced trend, with the largest value registered for W75P25. However, calculated values are very low (*ca.* 7–11 nm), thus suggesting a multicrystallinity in the systems. Vice versa, regarding the hematite crystal phase, the majority of the samples showed an average crystallite size remarkably larger than magnetite/maghemite phase (average size of *ca.* 70–85 nm). Interestingly, the only exception observed is the W25P75 sample, which presents a decrease in the average crystallite size (*ca.* 60 nm).

From the mechanistic viewpoint, Li et al. [48] investigated the stability of magnetite crystal phase under hydrothermal conditions by varying the temperature of treatment in the 120–275 °C range in presence of air-derived dissolved oxygen occupying the above part of the hydrothermal solution and ammonium hydroxide as alkaline medium. Authors evidenced different reaction mechanisms according to the temperature conditions. Between 120 and 180 °C, they registered the formation of maghemite (as intermediate oxidation product) through the solid state outward diffusion of ferrous ions (or inward diffusion of oxygen) with formation of a core/shell structure made of magnetite/maghemite with the oxidation of ferrous ions at the particle surfaces by O_2 (*i.e.*, with formation of a maghemite layer), along with the dissolution of maghemite, formation of aqueous ferric species (*e.g.*, ferric hydroxide) and precipitation of hematite. At 275 °C, instead, the hematite is directly formed on the magnetite uncovered surface [48]. In the present study, since we performed the synthesis maintaining constant the experimental condition (*i.e.*, temperature at 150 °C and reaction time 24 h), we can assume that more probably the oxidation mechanism involved is the maghemite-mediated route driven by the outward diffusion of ferrous ions from magnetite/maghemite within the

mixed solvent solution with subsequent oxidation of ferrous ions at the particle surfaces by means of dissolved O_2. In this context, it is expected that the different polarity of the mixed environment can favor/disfavor the dissolution of the iron oxide crystal phase and the solubility of Fe ions and dissolved oxygen in the medium, but further studies are necessary to clarify this point.

3.2. Magnetic characterizations

The magnetic properties of all synthesized samples were evaluated by means of VSM magnetization curves performed at RT. Magnetic parameters considered in the following are the magnetization curve profile, the magnetization value measured at the maximum investigated H field range (M_{max}), the remnant magnetization (M_r), and the coercivity (H_c). Fig. 5 illustrates the magnetization curves of all samples, which exhibited a very slight magnetic hysteresis. The maximum magnetization (M_{max}), remnant magnetization (M_r), and coercivity (H_c) values of all samples were summarized in Table 2. In particular, the differences observed in all samples could be directly correlated to both morphological and compositional variation [36].

According to the literature, at RT both magnetite and maghemite are ferrimagnetic substrates, with possibility of presenting a superparamagnetic behavior depending on particle size (*i.e.*, below *ca.* 20 nm size), whereas hematite crystal phase is either antiferromagnetic or strong paramagnetic material, depending on particle size and temperature [23,49–51].

In the case of the W100P0 sample, the magnetic characterization evidenced a M_{max} value of *ca.* 12.22 emu g^{-1} with a narrow hysteresis loop (with negligible M_r, and H_c values). This behavior is probably due to the prevalence of magnetite/maghemite crystal phase, which is known for being superparamagnetic in the case of small particles behaving as a single magnet, below *ca.* 20 nm in size [52]. By addition of 2-propanol into the synthesis medium (W75P25), a slight decrease of the M_{max} value to *ca.* 11.37 emu g^{-1} was registered, and an increase in both M_r and H_c values [53]. The highest values in terms of M_{max}, M_r, and H_c values were observed for the W50P50 sample, characterized by the presence of high content of magnetite/maghemite crystal phase (*ca.* 66 %). By further increasing the content of hematite, there was a progressive reduction of the M_{max} values from W25P75 (*ca.* 9 emu g^{-1}) to W0P100 samples (*ca.* 8 emu g^{-1}). These results agreed with the previously discussed data, thus indicating that the reaction environment selected for the synthesis played not only a significant role in the phase stabilization, but it also influenced the final magnetic properties.

Table 2
Magnetic parameters associated to the VSM magnetization curves profile of the synthesized samples measured at RT.

Sample	M_{max} (emu g^{-1})	M_r (emu g^{-1})	H_c (Oe)
W100P0	12.22	0.002	0.24
W75P25	11.37	0.007	1.53
W50P50	12.42	0.022	4.20
W25P75	9.28	0.011	2.61
W0P100	8.15	0.009	2.42

However, it should be pointed out that other effects can influence the magnetic properties such as the products purity, size and shape effects, as well as some surface effects, thus making a direct correlation between the nanomaterial characteristics and its magnetic response not easy to be rationalized.

According to the literature, Xu et al. [54] studied the influence of morphology variations in hematite nanoparticles with hexagonal microdisks, drum-like particles, spindles, and irregular shapes. These authors observed that the solvent medium adopted in their synthesis protocols (*i.e.*, a mixture of ethylene glycol and water) played a key role in both magnetite formation and in the hematite shape evolution, where high volume ratio of glycol (*i.e.*, ethylene glycol:water (3:1)) favored the formation of the hematite phase over the magnetite phase, probably due to the ethylene glycol reductive ability. Furthermore, the authors found that even the particle morphology affected the overall magnetic behavior of the iron oxide mixture, with the H_c values following the order hexagonal microdisks > drum-like particles > irregular particles > spindles, and the M_r values following almost the opposite order spindles > drum-like particles > irregular particles > hexagonal microdisks, respectively. Additionally, in our previous study [23], we reported the VSM magnetization curves profile for samples constituted by a mixture of magnetite/maghemite and hematite crystal phases with comparable composition (but different morphologies) showed analogous magnetization curve profiles and comparable magnetic parameters as the ones measured in the present study.

Therefore, a comprehensive evaluation of the morphological, structural, and magnetic characterizations indicated that:

1) W100P0 sample (with the highest content in the magnetite/maghemite crystal phase, *ca.* 70 %) presented the lowest H_c and M_r values (almost negligible) and a high M_{max} value compared to the other samples.

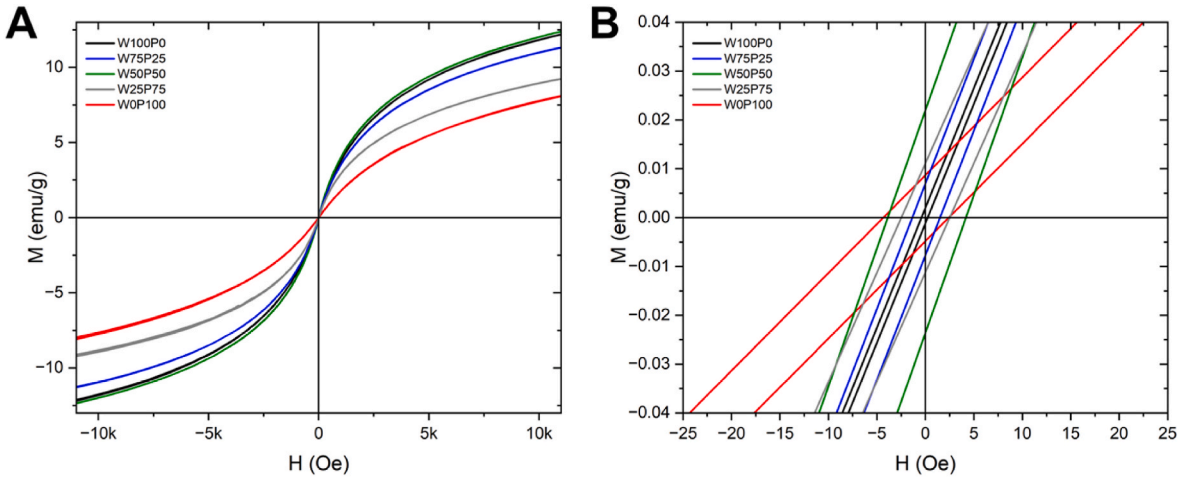

Fig. 5. Magnetization curves M vs. H of samples obtained in pure water environment, pure 2-propanol environment, and mixed water/2-propanol environment, varying the water/2-propanol volume ratio, namely: W100P0 (black), W75P25 (blue), W50P50 (green), W25P75 (grey), W0P100 (red). Panel (A) Magnetization curves full scale view. Panel (B) Magnetization curves enlargement area to highlight the middle section of the hysteresis loop. (For interpretation of the references to colour in this figure legend, the reader is referred to the Web version of this article.)

2) By decreasing the water/2-propanol volume ratio during synthesis, an enhancement of the hematite formation was observed, leading to a decrease in the M_{max} value. The only exception was the W50P50 sample, which showed the highest M_{max} (*ca.* 12.42 emu g^{-1}), H_c, and M_r values.
3) Both W25P75 and W0P100 samples had a comparable phase composition and similar magnetic behavior.

4. Conclusions

Noticeable variations in morphology and crystalline phase composition were obtained employing a mixed hydro-solvothermal protocol of synthesis for the production of iron oxide materials working at mild conditions (150 °C), using a mixed water/2-propanol reaction medium, and NaOH as precipitating agents.

The experimental results highlighted that, by varying the water/2-propanol volume ratio, it was possible to tune the particle shape, size, and crystal phase composition. In particular, results indicated that syntheses carried out at high water/2-propanol volume ratio promoted the predominant formation of the magnetite/maghemite crystal phase, whereas low water/2-propanol volume ratio favored the formation of the hematite crystal phase. The magnetic characterizations performed on the iron oxide-based samples pointed out the occurrence of slight magnetic hysteresis, with a gradual decrease in the M_{max} values as the water/2-propanol volume ratio decreased. Interestingly, the highest M_{max}, M_r, and H_c values were observed for the W50P50 sample. These results, although preliminary, are very promising, as they demonstrated the possibility to finely tailor both structural and functional (*i.e.*, magnetic) properties of iron oxide-based materials by simply varying the mixed hydro-solvothermal synthesis conditions, thus providing valuable insights for the rational design of mixed phase materials.

CRediT authorship contribution statement

Tatiana Rodríguez Flores: Writing – review & editing, Writing – original draft, Investigation, Formal analysis. **Falak Shafiq:** Writing – review & editing, Writing – original draft, Investigation, Formal analysis. **Gabriele Bona:** Writing – review & editing, Investigation, Formal analysis. **Giulia Bragaggia:** Writing – review & editing, Investigation. **Matteo Cantoni:** Writing – review & editing, Supervision, Resources, Investigation, Formal analysis. **Roberto Scotti:** Writing – review & editing, Investigation. **Silvia Gross:** Writing – review & editing, Supervision, Resources, Investigation, Formal analysis, Conceptualization. **Roberto Nisticò:** Writing – review & editing, Writing – original draft, Supervision, Resources, Investigation, Formal analysis, Conceptualization.

Data availability statement

Data will be made available on request.

Declaration of competing interest

The authors declare that they have no known competing financial interests or personal relationships that could have appeared to influence the work reported in this paper.

Acknowledgements

This work received financial support from MUR (Italy) and the European Union – Next Generation EU, Mission 4, Component 1, CUP (H53D23004490001) through the PRIN Project MAPEC (N. 2022599NR3), and CUP (H53D23008000001) through the PRIN Project PERFECT (N. P2022TK9B9). University of Milano-Bicocca is gratefully acknowledged for funding project Premio Giovani Talenti 2022. T.R.F. would like to acknowledge the Secreteria de Educacion, Ciencia, Tecnologia e Inovacion (Mexico City, Mexico) No. SECTEI/197/2024. The magnetic characterization was performed at Polifab, the micro and nanofabrication facility of Politecnico di Milano. Authors would like to acknowledge Dr. Paolo Gentile (University of Milano-Bicocca, Italy) for the technical support during the SEM analysis.

Abbreviations

H_c	coercivity
M_{max}	maximum magnetization
M_r	remnant magnetization
P’	Rohrschneider’s polarity parameter
RT	room temperature
SEM	scanning electron microscopy
VSM	vibrating sample magnetometry
XRPD	X-ray powder diffraction

References

[1] J. Tuček, K.C. Kemp, K.S. Kim, R. Zboril, Iron-oxide-supported nanocarbon in lithium-ion batteries, medical, catalytic, and environmental applications, ACS Nano 8 (2014) 7571–7612, https://doi.org/10.1021/nn501836x.
[2] S. Tanaka, Y.V. Kaneti, N.L.W. Septiani, S.X. Dou, Y. Bando, M.S.A. Hossain, J. Kim, Y. Yamauchi, A review on iron oxide-based nanoarchitectures for biomedical, energy storage, and environmental applications, Small Methods 3 (2019) 1800512, https://doi.org/10.1002/smtd.201800512.
[3] M.S. Bakshi, Iron oxide nanomaterials at interfaces for sustainable environmental applications, Acc. Mater. Res. 5 (2024) 1000–1012, https://doi.org/10.1021/accountsmr.4c00151.
[4] K. Ansari, R. Ahmad, M.S. Tanweer, I. Azam, Magnetic iron oxide nanoparticles as a tool for the advancement of biomedical and environmental application: a review, Biomed. Mater. Devices 2 (2024) 139–157, https://doi.org/10.1007/s44174-023-00091-y.
[5] G. Bona, L. Viganò, M. Cantoni, R. Mantovan, B. Di Credico, S. Mostoni, R. Scotti, R. Nisticò, An experimental demonstration on the recyclability of hybrid magnetite-humic acid nanoparticles, Sustain. Mater. Technol. 43 (2025) e01275, https://doi.org/10.1016/j.susmat.2025.e01275.
[6] W. Wu, C. Jiang, V.A.L. Roy, Recent progress in magnetic iron oxide–semiconductor composite nanomaterials as promising photocatalysts, Nanoscale 7 (2015) 38–58, https://doi.org/10.1039/C4NR04244A.
[7] V. Polliotto, F.R. Pomilla, V. Maurino, G. Marcì, A. Bianco Prevot, R. Nisticò, G. Magnacca, M.C. Paganini, L. Ponce Robles, L. Perez, S. Malato, Different approaches for the solar photocatalytic removal of micro-contaminants from aqueous environment: Titania vs. hybrid magnetic iron oxides, Catal. Today 328 (2019) 164–171, https://doi.org/10.1016/j.cattod.2019.01.044.
[8] P. Kumar, N. Thakur, K. Kumar, S. Kumar, A. Dutt, V.K. Thakur, C. Gutiérrez-Rodelo, P. Thakur, A. Navarrete, N. Thakur, Catalyzing innovation: exploring iron oxide nanoparticles - origins, advancements, and future application horizons, Coord. Chem. Rev. 507 (2024) 215750, https://doi.org/10.1016/j.ccr.2024.215750.
[9] P. Rajiv, R. Manikandan, S. Sangeetha, P. Vanathi, S. Dhanasekaran, Fabrication of biogenic iron oxide and their efficiency to detect carbofuran in vegetable samples, Inorg. Chem. Commun. 142 (2022) 109649, https://doi.org/10.1016/j.inoche.2022.109649.
[10] A. Ghazzy, H. Nsairat, R. Said, O.A. Sibai, A. AbuRuman, A.S. Shraim, A. Al Hunaiti, Magnetic iron oxide-based nanozymes: from synthesis to application, Nanoscale Adv. 6 (2024) 1611–1642, https://doi.org/10.1039/D3NA00903C.
[11] A. Chauhan, G. Rana, V. Dutta, A. Kumari, S.K. Rao, R. Subbarayan, K. Ravi, S. Selvaraj, S. Ghotekar, Recent trends in phyto-mediated iron-based nanomaterials for environmental remediation and biomedical applications, Inorg. Chem. Commun. 160 (2024) 111976, https://doi.org/10.1016/j.inoche.2023.111976.
[12] A. Valizadeh, A. Mirzapoor, Z. Hallaji, M.J. Talab, B. Ranjbar, Innovative synthesis of magnetite nanoparticles and their interaction with two model proteins: human serum albumin and lysozyme, Part. Part. Syst. Char. 42 (2025) 2400168, https://doi.org/10.1002/ppsc.202400168.
[13] S. Zhang, Z. Deng, B. Yao, J. Wu, Z. Jiao, N. Gu, Polyhedral magnetic nanoparticles of high magnetization synthesized by hydrocooling and magnetically internal heating coprecipitation: implications for magnetic resonance imaging, ACS Appl. Nano Mater. 7 (2024) 10377–10386,, https://doi.org/10.1021/acsanm.4c00833.
[14] Z.R. Stephen, F.M. Kievit, M. Zhang, Magnetite nanoparticles for medical MR imaging, Mater. Today 14 (2011) 330–338, https://doi.org/10.1016/S1369-7021(11)70163-8.
[15] S.J. Olusegun, M. Osial, A. Majkowska-Pilip, K. Żelechowska-Matysiak, D. Nieciecka, M. Krajewski, M. Pękała, P. Krysinski, Synthesis and characterization of Sr^{2+} and Gd^{3+} doped magnetite nanoparticles for magnetic hyperthermia and drug delivery application, Ceram. Int. 49 (2023) 19851–19860, https://doi.org/10.1016/j.ceramint.2023.03.102.
[16] F. Caldera, R. Nisticò, G. Magnacca, A. Matencio, Y.K. Monfared, F. Trotta, Magnetic composites of dextrin-based carbonate nanosponges and iron oxide

nanoparticles with potential application in targeted drug delivery, Nanomaterials 12 (2022) 754, https://doi.org/10.3390/nano12050754.
[17] F. Cesano, G. Fenoglio, L. Carlos, R. Nisticò, One-step synthesis of magnetic chitosan polymer composite films, Appl. Surf. Sci. 345 (2015) 175–181, https://doi.org/10.1016/j.apsusc.2015.03.154.
[18] M. Tadic, J. Lazovic, M. Panjan, B.V. Tadic, Y. Lalatonne, Solvothermal synthesis of hematite (α-Fe_2O_3) nanoparticles: influence of surfactants on morphology, magnetic anisotropy, MRI relaxivity and biocompatibility, Inorg. Chem. Commun. 176 (2025) 114290, https://doi.org/10.1016/j.inoche.2025.114290.
[19] S. Ahmad, M. Khan, S.B. Khan, A.M. Asiri. Effect of cobalt-doped iron oxide as an electrocatalyst for water splitting and photocatalytic hydrogen evolution. Inorg. Chem. Commun. 170. 2924, 113421. 10.1016/j.inoche.2024.113421.
[20] R. Nisticò, A synthetic guide toward the tailored production of magnetic iron oxide nanoparticles, Bol. Soc. Esp. Ceram. V 60 (2021) 29–40, https://doi.org/10.1016/j.bsecv.2020.01.011.
[21] C. Sanchez, L. Rozes, F. Ribot, C. Laberty-Robert, D. Grosso, C. Sassoye, C. Boissiere, L. Nicole, "Chimie douce": a land of opportunities for the designed construction of functional inorganic and hybrid organic-inorganic nanomaterials, C. R. Chim. 13 (2010) 3–39, https://doi.org/10.1016/j.crci.2009.06.001.
[22] S. Diodati, R.I. Walton, S. Mascotto, S. Gross, Low-temperature wet chemistry synthetic approaches towards ferrites, Inorg. Chem. Front. 7 (2020) 3282–3314, https://doi.org/10.1039/D0QI00294A.
[23] G. Bona, G. Bragaggia, M. Cantoni, B. Di Credico, S. Mostoni, G. Capitani, R. Scotti, S. Gross, R. Nisticò, Polyethylene glycol-assisted hydro-solvothermal growth of anisotropic magnetic iron oxides: the role of mixed environment conditions, Colloids Surf. A Physicochem. Eng. Asp. 702 (2024) 135117, https://doi.org/10.1016/j.colsurfa.2024.135117.
[24] G. Demazeau, Solvothermal and hydrothermal processes: the main physico-chemical factors involved and new trends, Res. Chem. Intermed. 37 (2011) 107–123, https://doi.org/10.1007/s11164-011-0240-z.
[25] B.S. Wu, P. Wang, J. Song, Mixed-solvothermal synthesis and morphology-dependent electrochemical properties of α-Fe_2O_3 nanoparticles for lithium-ion batteries, J. Mater. Sci. Mater. Electron. 31 (2020) 6779–6785, https://doi.org/10.1007/s10854-020-03236-7.
[26] Y. Zhang, C. Li, L. Liu, K. Wang, Y. Zhu, J. Ben, J. Wu, Solvothermal synthesis of mesoporous Fe_3O_4 nanoparticles in mixed solvent of ethylene glycol and water: structure and magnetic properties, J. Supercond. Nov. Magn. 32 (2019) 757–762, https://doi.org/10.1007/s10948-018-4766-9.
[27] T. Xin, M. Ma, H. Zhang, J. Gu, S. Wang, M. Liu, Q. Zhang, A facile approach for the synthesis of magnetic separable Fe_3O_4@TiO_2, core–shell nanocomposites as highly recyclable photocatalysts, Appl. Surf. Sci. 288 (2014) 51–59, https://doi.org/10.1016/j.apsusc.2013.09.108.
[28] J. Wang, Q. Chen, B. Hou, Z. Peng, Synthesis and magnetic properties of single-crystals of $MnFe_2O_4$ nanorods, Eur. J. Inorg. Chem. 2004 (2004) 1165–1168, https://doi.org/10.1002/ejic.200300555.
[29] S. Mahadevan, G. Gnanaprakash, J. Philip, B.P.C. Rao, T. Jayakumar, X-ray diffraction-based characterization of magnetite nanoparticles in presence of goethite and correlation with magnetic properties, Phys. E: Low-Dimens. Syst. Nanostructures 39 (2007) 20–25, https://doi.org/10.1016/j.physe.2006.12.041.
[30] R.F. Karlak, D.S. Burnett, Quantitative phase analysis by X-ray diffraction, Anal. Chem. 38 (1966) 1741–1745, https://doi.org/10.1021/ac60244a026.
[31] W. Kim, C.Y. Suh, S.W. Cho, K.M. Roh, H. Kwon, K. Song, I.J. Shon, A new method for the identification and quantification of magnetite–maghemite mixture using conventional X-ray diffraction technique, Talanta 94 (2012) 348–352, https://doi.org/10.1016/j.talanta.2012.03.001.
[32] H. Itoh, T. Sugimoto, Systematic control of size, shape, structure, and magnetic properties of uniform magnetite and maghemite particles, J. Colloid Interf. Sci. 265 (2003) 283–295, https://doi.org/10.1016/S0021-9797(03)00511-3.
[33] N. Torres-Gómez, O. Nava, L. Argueta-Figueroa, R. García-Contreras, A. Baeza-Barrera, A.R. Vilchis-Nestor, Shape tuning of magnetite nanoparticles obtained by hydrothermal synthesis: effect of temperature, J. Nanomater. 15 (2019) 79212739, https://doi.org/10.1155/2019/7921273.
[34] D.B. Kargin, Y.V. Konyukhov, A.B. Biseken, A.S. Lileev, D. Yu Karpenkov, Structure, morphology and magnetic properties of hematite and maghemite nanopowders produced from rolling mill scale, Steel Transl. 50 (2020) 151–158, https://doi.org/10.3103/S0967091220030055.
[35] M. Ashraf, I. Khan, M. Usman, A. Khan, S.S. Shah, A.Z. Khan, K. Saeed, M. Yaseen, M.F. Ehsan, M.N. Tahir, N. Ullah, Hematite and magnetite nanostructures for green and sustainable energy harnessing and environmental pollution control: a review, Chem. Res. Toxicol. 33 (2020) 1292–1311, https://doi.org/10.1021/acs.chemrestox.9b00308.
[36] I.M. Grabs, C. Bradtmöller, D. Menzel, G. Garnweitner, Formation mechanisms of iron oxide nanoparticles in different nonaqueous media, Cryst. Growth Des. 12 (2012) 1469–1475, https://doi.org/10.1021/cg201563h.
[37] P.R. Sajanlal, T.S. Sreeprasad, A.K. Samal, T. Pradeep, Anisotropic nanomaterials: structure, growth, assembly, and functions, Nano Rev. 2 (2011) 5883, https://doi.org/10.3402/nano.v2i0.5883.
[38] R.C. Pawar, J.H. Um, S. Kang, W.-S. Yoon, H. Choe, C.S. Lee, Solvent-polarity-induced hematite (α-Fe_2O_3) nanostructures for lithium-ion battery and photoelectrochemical applications, Electrochim. Acta 245 (2017) 643–653, https://doi.org/10.1016/j.electacta.2017.05.070.
[39] D.R. Modeshia, R.I. Wilson, Solvothermal synthesis of perovskites and pyrochlores: crystallisation of functional oxides under mild conditions, Chem. Soc. Rev. 39 (2010) 4303–4325, https://doi.org/10.1039/B904702F.
[40] N.K. Chaudhari, H.C. Kim, C.S. Kim, J. Park, J.-S. Yu, Solvent controlled synthesis of new hematite superstructures with large coercive values, CrystEngComm 14 (2012) 2024–2031, https://doi.org/10.1039/C1CE06444D.
[41] L. Yu, R. Han, X. Sang, J. Liu, M.P. Thomas, B.M. Hudak, A. Patel, K. Page, B. S. Guiton, Shell-induced ostwald ripening: simultaneous structure, composition, and morphology transformations during the creation of hollow iron oxide nanocapsules, ACS Nano 12 (2018) 9051–9059, https://doi.org/10.1021/acsnano.8b02946.
[42] Shodex.com. Polarities of Solvents. Available at: https://www.shodex.com/en/dc/06/0117.html (accessed on July 31, 2025).
[43] X. Lu, M. Li, S. Hoang, S.L. Suib, P.-X. Gao, Solvent effects on the heterogeneous growth of TiO_2 nanostructure arrays by solvothermal synthesis, Catal. Today 360 (2021) 275–283, https://doi.org/10.1016/j.cattod.2020.02.044.
[44] Y. He, Y. Zhu, N. Wu, Mixed solvents: a key in solvothermal synthesis of $KTaO_3$, J. Solid State Chem. 177 (2004) 2985–2990, https://doi.org/10.1016/j.jssc.2004.04.051.
[45] J. Zhao, J. Brugger, A. Pring, Mechanism and kinetics of hydrothermal replacement of magnetite by hematite, Geosci. Front. 10 (2019) 29–41, https://doi.org/10.1016/j.gsf.2018.05.015.
[46] M. Satheesh, A.R. Paloly, K.G. Suresh, M.J. Bushiri, Influence of solvothermal growth condition on morphological formation of hematite spheroid and pseudocubic micro structures and its magnetic coercivity, J. Phys. Chem. Solid. 98 (2016) 247–254, https://doi.org/10.1016/j.jpcs.2016.07.020.
[47] A. An, J. Zhang, S. Pan F. Yu, Facile template-free synthesis and characterization of elliptic α-Fe_2O_3 superstructures, J. Phys. Chem. C 113 (2009) 8092–8096, https://doi.org/10.1021/jp9004168.
[48] Z. Li, C. Chaneac, G. Berger, S. Delaunay, A. Graff, G. Lefevre, Mechanism and kinetics of magnetite oxidation under hydrothermal conditions, RSC Adv. 9 (2019) 33633–33642, https://doi.org/10.1039/C9RA03234G.
[49] S.H. Lafta, Evaluation of hematite nanoparticles weak ferromagnetism, J. Supercond. Nov. Magn. 33 (2020) 3765–3772, https://doi.org/10.1007/s10948-020-05626-8.
[50] M. Tadic, J. Lazovic, M. Panjan, B.V. Tadic, Y. Lalatonne, Low-coercivity behavior and biomedical potential of cube-like and rounded hematite (α-Fe_2O_3) nanoparticles: insights from hydrothermal synthesis, Mater. Sci. Eng. B 317 (2025) 118204, https://doi.org/10.1016/j.mseb.2025.118204.
[51] M. Tadić, Z. Jagličić, J. Lazović, S. Nemec, S. Kralj, SPION clusters with porous silica shell: synthesis, core-shell structure, magnetic properties, biocompatibility and MRI application, Ceram. Int. 51 (2025) 15521–15534, https://doi.org/10.1016/j.ceramint.2025.01.388.
[52] A.S. Teja, P.Y. Koh, Synthesis, properties, and applications of magnetic iron oxide nanoparticles, Prog. Cryst. Growth Charact. Mater. 55 (2009) 22–45, https://doi.org/10.1016/j.pcrysgrow.2008.08.003.
[53] H. Hu, Y. Yuan, S. Lim, C.H. Wang, Phase structure dependence of magnetic behaviour in iron oxide nanorods, Mater. Des. 185 (2020) 108241, https://doi.org/10.1016/j.matdes.2019.108241.
[54] G. Xu, L. Li, Z. Shen, Z. Tao, Y. Zhang, H. Tian, X. Wei, G. Shen, G. Han, Magnetite Fe_3O_4 nanoparticles and hematite α-Fe_2O_3 uniform oblique hexagonal microdisks, drum-like particles and spindles and their magnetic properties, J. Alloys Compd. 629 (2015) 36–42, https://doi.org/10.1016/j.jallcom.2014.11.140.